Journal of
Synchrotron
Radiation

ISSN 0909-0495

Received 26 June 2012
Accepted 25 September 2012

Electronic structure and hybridization of CaS by means of X-ray absorption spectroscopy at Ca and S *K*-edges

Wei Xu,[a]* Lijuan Liu,[a] Mingqi Cui,[a] Lei Zheng,[a] Yongfeng Hu,[b] Augusto Marcelli[a,c] and Ziyu Wu[d]*

[a]Insitute of High Energy Physics, Chinese Academy of Sciences, Beijing 100049, People's Republic of China, [b]Canadian Light Source, University of Saskatchewan, Saskatoon, Canada, [c]Laboratori Nazionali di Frascati, Istituto Nazionale di Fisica Nucleare, 00044 Frascati, Italy, and [d]National Synchrotron Radiation Laboratory, University of Science and Technology of China, Hefei 230026, People's Republic of China. E-mail: xuw@mail.ihep.ac.cn, wuzy@ustc.edu.cn

The cubic calcium sulfide (CaS) is a well known system and an attractive building block material for many luminescence technological applications. However, it is essential to achieve an accurate understanding of its electronic structure in order to engineer its band structure for optimized applications. Here a study of the electronic structure of CaS by means of X-ray absorption spectroscopy performed at both Ca and S *K*-edges, and calculations performed in the framework of the multiple-scattering theory and of the finite difference method are presented. At the Ca *K*-edge the presence of an anomalous *d* states feature is discussed while in the S *K*-edge spectrum the presence of a pre-edge shoulder owing to the hybridization among Ca *d* states and S *p* states is pointed out. Although the *l*-projected density of states of CaS is in good agreement with previous first-principles calculations, the standard muffin-tin potential is inadequate to reproduce near-edge structures at both Ca and S *K*-edges in this system. Indeed, with its highly symmetric and less compact structure, CaS is characterized by a large set of collinear atomic configurations that pose severe constraints on the construction of the atomic potential. On the contrary, the finite-difference method with no muffin-tin approximation is more suitable for X-ray absorption calculations in this system.

Keywords: CaS; X-ray absorption spectroscopy; Ca *K*-edge; S *K*-edge.

1. Introduction

Calcium sulfide (CaS) (Fig. 1) has a typical cubic crystal structure, with space group $Fm\bar{3}m$ (No. 225) and large unit cell of 5.68 Å. Owing to the wide band-gap (~5.38 eV), CaS is technologically important as a host material in luminescence technology (Rao, 1986; Versluys *et al.*, 2001; Hakamata *et al.*, 2005; Barrett *et al.*, 2005). Meanwhile, it also exhibits unique structural behavior under high pressure. At room temperature and ambient pressure CaS has the NaCl-type (B1) structure but at high pressure, above 40 GPa, the crystal structure transforms into the CsCl-type (B2) (Luo *et al.*, 1994). B2–B4 (wurtzite) and B2–B3 (zinc blende) phase transitions have also been predicted (Chen *et al.*, 2007) to occur at low pressure, around 0.829 GPa and 0.679 GPa, respectively. Theoretical calculations based on density functional theory have been successfully employed to calculate the electronic structure, optical properties and thermodynamic parameters (Chen *et al.*, 2007; Shaukat *et al.*, 2008; Guo *et al.*, 2008). The electronic structure varies with the type of exchange-correlation potential functional (Shaukat *et al.*, 2008).

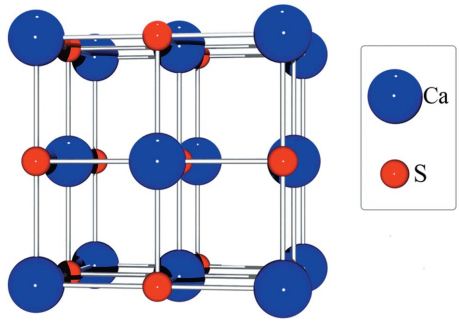

Figure 1
Sketch of the cubic crystal structure of calcium sulfide, whose symmetry group is $Fm\bar{3}m$ (No. 225) with a = 5.686 Å. The nearest-neighboring atomic distance between Ca and S atoms is 2.8 Å, suggesting a less compact lattice structure.

Furthermore, X-ray absorption spectroscopy is a recognized local structure and element-selective probe to study electronic structures, widely used in different fields. Absorption spectroscopy at intermediate energies is experiencing continuously increasing interest, not only for the easy availability now offered by modern X-ray beamlines but also because the elements with edges falling in this energy regime are non-toxic light elements such as calcium, potassium, sulfur, *etc.* For instance, the sulfides including CaS were investigated extensively by X-ray absorption spectroscopy at the sulfur *K*-edge and $L_{2,3}$-edge, respectively (Farrell *et al.*, 2002; Kravtsova *et al.*, 2004). Owing to the improvement of energy resolution, the experimental spectrum can be measured with detailed features (Alonso Mori *et al.*, 2009). On the other hand, theoretical simulation of XANES spectra is improved by either using the muffin-tin (MT) method with a constant potential in the interstitial region among atoms, or with a full potential with no boundaries. To justify the electronic structure, it is essential to investigate the potential effects that may exist in some open structure (Xu *et al.*, 2011). The combination of advanced analytical tools and the improved experiment allows us to improve the interpretation of the electronic structure of CaS. Therefore, the major motivation of this research is the optimization at mid-energy of X-ray absorption spectroscopy calculations by comparing conventional MT and non-MT potentials within the framework of the multiple-scattering theory (MST). We will explore the system at two different edges, *i.e.* the Ca *K*-edge and S *K*-edge, which may provide a more comprehensive overview of the electronic structure. To the best of our knowledge, this is the first attempt to perform an accurate comparison of XAS simulations at intermediate energy, though a previous work at the potassium *K*-edge has already partially faced up the potential issue in micas (Xu *et al.*, 2011). It is worth mentioning here that the CaS system is highly symmetric with a cubic symmetry and a small unit cell containing only two atoms. This configuration is extremely different from micas, a system characterized by a low symmetry and a much larger unit cell (>20 inequivalent atoms). An additional goal of this work is then identifying limitations of the MT potential at different absorption edges, in order to provide evidence for refinement of XAS theory.

2. Experiment

The CaS powder with a purity of 99.9% was purchased from Alfa Aesar. X-ray absorption spectra at both Ca and S *K*-edges were collected at the 06B1-1 (SRXMB) beamline at the Canadian Light Source. The incident energy was tuned by a Si (111) double-crystal monochromator characterized by a theoretical energy resolution of 0.24 eV and 0.4 eV at the S and Ca *K*-edges, respectively. The total-electron-yield (TEY) mode was employed to collect spectra. For the following analysis a linear background was subtracted from the raw data and spectra were then normalized to the edge step by using the *IFEFFIT* package (Ravel & Newville, 2005).

3. Theoretical calculations

To interpret X-ray near-edge absorption spectra, we performed theoretical calculations in the framework of the MST within the MT potential approximation and the finite difference method with a full potential. Both methods were implemented in the *FDMNES(2012)* code (Joly, 2001). The non-MT calculation was performed by constructing a grid of order 4, with an inter-point distance equal to 0.25 Å within a cluster radius of 0.65 Å. A discretization of the Schrödinger-like equation at finite points of this grid was considered. For MT calculations, two types of clusters with radii of 8 Å and 12 Å were adopted to calculate the self-consistent potential as well as XANES spectra. Clusters with radii of 7 Å and 12 Å were employed for non-MT calculations. The starting unit-cell parameter for the cubic CaS B1 ($Fm\bar{3}m$, No. 225) structure is 5.68 Å. The final converging cluster size was 12 Å wide and contained 305 atoms around the central absorber for both S and Ca atoms. Meanwhile, we compared the *FEFF9.0* code (Rehr *et al.*, 2009) that employs the real-space Green's function method in the framework of the MST but with a self-consistent MT potential. The Hedin–Lundqvist (Hedin & Lundqvist, 1970) exchange-correlation potential was used and a cluster radius of 5 Å was adopted to construct the self-consistent potential. The radius of the full multiple-scattering cluster was also 12 Å and the projected density of states was obtained using the *FEFF9.0* code. Note that all calculations (*FEFF* and *FDMNES*) employed self-consistent potential.

4. Results and discussions

Both *FEFF* and *FDMNES* codes employ Green's function to construct the transition matrix and the absorption cross sections within the MT potential approximation in the framework of the full multiple-scattering theory (FMST). In order to illustrate the universality of these calculations, we performed MT FMST calculations with the same cluster size using both *FEFF* and Green's function mode of the *FDMNES* code. As shown in Figs. S1 and S2[1], calculations for a cluster with a radius of ~12 Å made with *FEFF* and *FDMNES* are quite similar at both Ca and S *K*-edges. However, a difference occurs in the near-edge region at the Ca *K*-edge, which is due to the different convolution function that accounts for the core-hole lifetime and the inelastic losses during the scattering process of electrons. The spectra also show that in this case the MT approach cannot reproduce experimental XANES spectra, especially in the near-edge region. In a previous MT calculation (Kravtsova *et al.*, 2004) the experimental spectrum was less resolved and not all features were reproduced. Owing to the low energy resolution at least one shoulder was smeared (Kravtsova *et al.*, 2004). Working at high spectral resolution, the recent measured XANES spectra (*e.g.* Ca *K*-edge) are characterized by a structured pre-edge not reproduced by MT potential methods. With a nearest-neighbor bond length

[1] Supplementary data for this paper are available from the IUCr electronic archives (Reference: HF5217). Services for accessing these data are described at the back of the journal.

Table 1
The MT radius (Å) of each atom determined using different procedures.

Edge	Atoms	10%[a]	12%[b]	15%[c]	Raydem[d]	Norman[e]
Ca *K*-edge	Ca (excited)	1.57115	1.57748	1.59408	1.56200	1.68396
	Ca (ground)	1.60065	1.61810	1.65075	1.56200	1.68808
	S	1.57793	1.57128	1.60065	1.56200‘	1.44004
S *K*-edge	S (excited)	1.44891	1.46090	1.47764	1.56200	1.40908
	S (ground)	1.58741	1.57128	1.60065	1.56200	1.43637
	Ca	1.60065	1.66104	1.69208	1.56200	1.71492

[a]10% refers to a 10% overlap of MT radius optimized to have the smallest potential discontinuity among atoms. [b]12% refers to a 12% overlap of MT radius optimized to have the smallest potential discontinuity among atoms. [c]15% refers to a 15% overlap of MT radius optimized to have the smallest potential discontinuity among atoms. [d]Raydem corresponds to a MT radius half of the interatomic distance. [e]Norman refers to the determination of the MT radius according to the Norman procedure, *i.e.* the radii around atoms are chosen to keep the spherically averaged charge within each radius equal to that of the neutral atom. An extra 10% overlap is introduced in this procedure.

of 2.84 Å, MT potentials are not able to properly reproduce the potential experienced by photoelectrons and a full potential approach is required. In the following sections we will discuss MT *versus* non-MT calculations at both Ca and S *K*-edges.

4.1. MT radius and potential effects

The nearest-neighbor interatomic distance in CaS is 2.84 Å and the lattice structure is not closely packed. It has already been pointed out that a MT potential is not optimized for an open structure (Rehr & Albers, 2000). As we will show next, by performing calculations with varying MT potentials and MT radii, this also holds true for the cubic CaS structure. Regarding the MT potential, the conventional way to construct the potential is by imposing a constant interstitial potential with either overlapping or non-overlapping MTs (Rehr & Albers, 2000). We analysed potential effects by changing the overlap value and determining the MT radius for the different procedures. In Table 1 we list the corresponding MT radii for each atom in the XANES calculations at the Ca and S *K*-edges. In the Norman procedure (Norman, 1974) the MT radius is determined so as to guarantee that the integral charge within the MT sphere is equal to the total atomic charge. An extra 10% overlap is introduced (Natoli *et al.*, 2003). In the Raydem approach the MT radius is arbitrarily defined as half of the interatomic distance. A third procedure optimizes the MT radii in order to minimize discontinuities at the boundaries. The overlap factor we considered (10%, 12% and 15%) will compensate for discontinuities between adjacent MT spheres (Joly, 2001).

Spectral difference among models with different MT radius determined from the aforementioned procedures and a model with a 10% overlap factor are compared for both Ca and S *K*-edges. In Figs. 2 and 3, spectral differences as well as spectra calculated with different MT radii are shown. Clearly the near-edge region shows differences for different MT radii; and the intensity of the pre-edge peak is much higher in the case of the Raydem and Norman procedures. In Table 1 the MT radii of atoms corresponding to different procedures are listed. Apparently, the MT radius of calcium as determined by the Norman procedure is larger than others while the MT radius of sulfur is slightly smaller. Remarkably, spectral variations with respect to different MT radii are distinctive of both Ca and S *K*-edges. At the Ca *K*-edge the 12% and 15% overlaps show similar spectral trends while the Raydem and Norman results belong to a different group with similar variation. As shown in

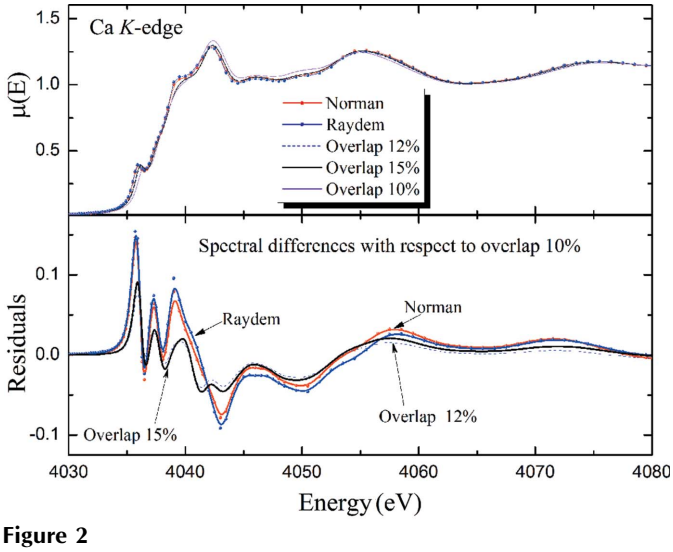

Figure 2
(Top) Comparison of Ca *K*-edge XANES spectra calculated with different MT radii (see text for more details on the procedure to determine the different MT radius). (Bottom) Spectral difference between each spectrum and a reference spectrum calculated with the MT radius with a 10% overlap. The red dotted line refers to the Norman procedure; the blue dotted line is the Raydem procedure; the blue dashed line correspond to a 12% overlap, the black solid line to a 15% overlap.

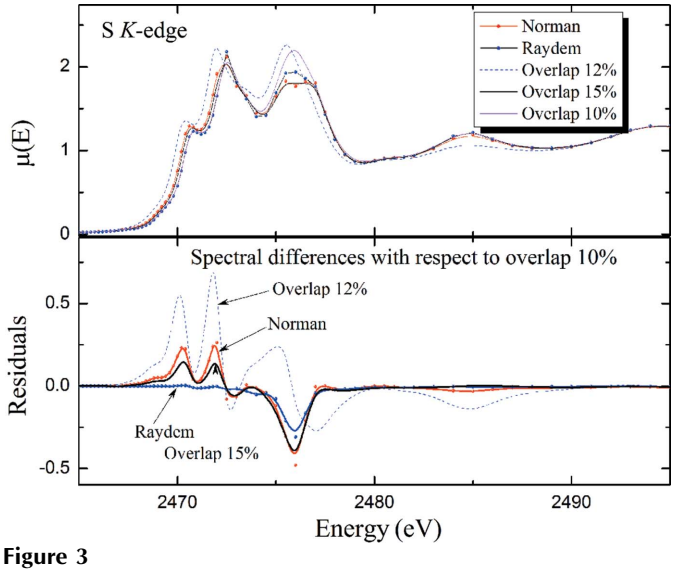

Figure 3
(Top) Comparison of S *K*-edge XANES spectra calculated with different MT radii (see text for more details on the procedure to determine the different MT radius). (Bottom) Spectral difference between each spectrum and a reference spectrum calculated with the MT radius with a 10% overlap. The red dotted line refers to the Norman procedure; the blue dotted line is the Raydem procedure; the blue dashed line correspond to a 12% overlap, the black solid line to a 15% overlap.

Table 1, the MT radius of the S atom in the first overlap set (12% and 15%) is larger than that of the second set (Raydem and Norman). Since the first-shell atoms around calcium are S atoms, their MT radii directly determine how much charge is contained in the small atomic cluster. The smaller sulfur MT radius and the larger one of Ca lead to an increased dispersion of sulfur *p* orbitals towards Ca *d* orbitals, in agreement with the observed intensity enhancement of the pre-edge feature at the Ca *K*-edge. Indeed, pre-edge features at the Ca *K*-edge originate from empty states of *d* character hybridized with *p* orbitals, as confirmed by density of states calculations presented in the following sections. The interpretation of spectral variations at the S *K*-edge is, on the contrary, not straightforward. S *K*-edge XANES changes dramatically *versus* the MT radius as determined by different procedures: (i) most of the spectral variations concentrate at the near-edge region from 2470 to 2480 eV, except for the case of the 12% overlap whose spectral variation extends over a larger energy range up to 30–40 eV above the edge; (ii) the Raydem case also shows significant spectral differences around 2476 eV, corresponding to the second peak of the structured edge; (iii) the spectral difference for 15% overlap is less relevant than the Norman one and of the 12% overlap, pointing out that the choice of the MT radius is much more critical at the S *K*-edge.

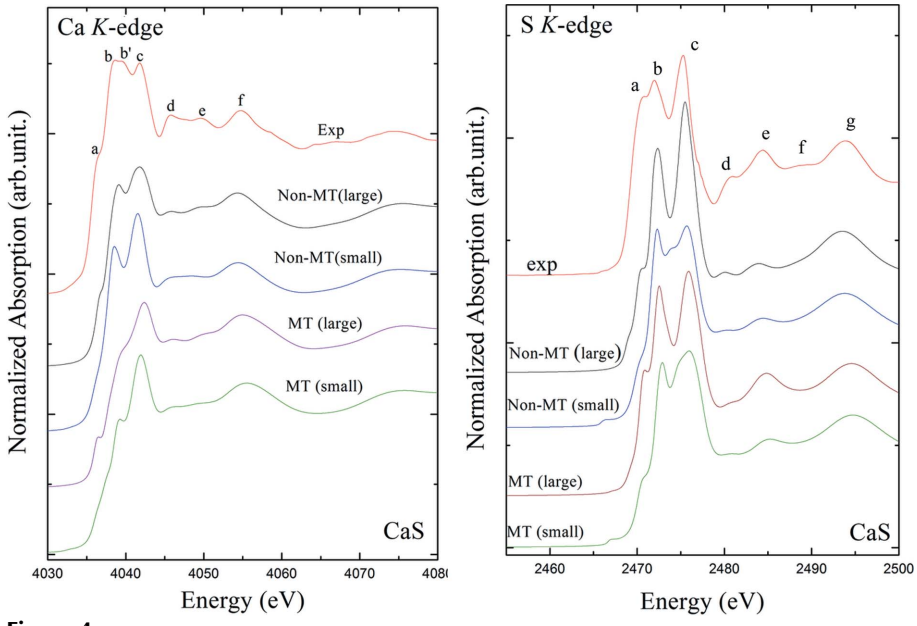

Figure 4
(Left) Comparison of Ca *K*-edge XANES spectra calculated for different cluster sizes and both MT and non-MT methods. (Right) The same as in the left panel but for the S *K*-edge.

To achieve semi-qualitative information, we compared the MT radius (Table 1) from different procedures simulating S *K*-edge XANES. For the excited sulfur, the Norman procedure generates the smallest MT radius (1.40908 Å) while the Raydem procedure produces the largest one (1.44891 Å). For S atoms in the ground state, the MT radius for 12% overlap is 0.02 Å shorter than that for 10% overlap. It implies that charged states penetrate into the Ca MT regions. Consequently, the MT radius of Ca is larger with 12% overlap than that with 10% overlap (Table 1). Moreover, the 12% overlap also induces a shift of the Fermi energy level that determines a threshold of empty and occupied states; therefore, there is a significant spectral difference between the 12% overlap and 10% overlap. It is already known that the Fermi energy determined from the MT potential approximation has an uncertainty of about 1 eV (Moreno *et al.*, 2007). In this case we point out that the Fermi energy is significantly affected by the selected MT radius for light elements such as sulfur. Although the MT approximation is trustworthy as tested in many different systems, the CaS system poses severe constraints to potential boundary conditions and the determination of the Fermi level is not straightforward. We ought to consider a non-MT potential to better understand the origin of the observed spectral variations that is probably induced by potential boundary effects.

4.2. Calcium *K*-edge: MT *versus* non-MT potential

In Fig. 4 (left), experimental and theoretical Ca *K*-edge XANES spectra of CaS are compared. Four types of theoretical spectra have been calculated to compare size effects induced by different cluster sizes and potential effects owing to MT *versus* non-MT approximations. The collinear alignment of atoms in the rock-salt cubic lattice generates long-range-order effects in CaS in both the Ca and S *K*-edge spectra. Actually, a long-range atomic arrangement (cluster of radius ∼12 Å) has to be considered as in a previous report (Kravtsova *et al.*, 2004). To study the potential effects we performed non-MT potential calculations using the same cluster size. It shall be underlined here that the non-MT method, *i.e.* the finite-difference method, is extremely time-consuming and computationally challenging. In this case, only two cluster sizes were attempted for the FDM method because of practical limitations.

Size effects at the Ca *K*-edge are evident for both MT and non-MT approaches. Specifically, the features *d* and *e* in Fig. 4 are more evident as the cluster radius increases from 8 Å to 12 Å. Therefore, the high-energy feature *e* originates from multiple-scattering contributions occurring in an outer sphere extending over the smaller radius. As mentioned above, pre-edge features at the Ca *K*-edge are closely related to the hybridization among Ca *d* states and S *p* states. Moreover, the Fermi energy level is also slightly affected by the size of the MT radii of each atom. Apparently the non-MT approach reproduces very well the Fermi energy and also the position of both the pre-edge feature *a* and the white-line *b*. Size effects

also determine unique behaviors in the XANES spectra of CaS: (i) the pre-edge peak (feature *a*), regardless of its position, appears in large clusters while it disappears in the smaller one, no matter whether MT or non-MT potentials are employed; (ii) the intensity of the white line (feature *c*) reduces in larger clusters, a behavior present in both MT and non-MT simulations. The feature *a* probes the hybridization among electron orbitals as well as long-rang-order scattering effects, while the feature *c* mainly mirrors the interference between different scattering waves from different atomic shells.

Neglecting the anomalous feature *b*′, in between the *b* and the *c* features, the non-MT approach reproduces experimental spectra quite well both in terms of peak positions and intensity. As for the feature *b*′, it probably probes an additional transition channel opened to electron transition. It may be a multiple electron excitation or an extra charge transfer from sulfur to calcium owing to radiation damage. In silicate glasses it has been observed that a fraction of S^{2-} changes to S^{4+} owing to radiation damage (Wilke *et al.*, 2008). Independently, data confirm that the MT approach is inadequate to describe the absorption spectrum at the Ca *K*-edge in CaS. Calculations could be improved by introducing a non-MT treatment of the potential, and using a large cluster to better reduce size effects.

4.3. Sulfur *K*-edge: MT *versus* non-MT potential

In this section we will describe potential and size effects at the S *K*-edge. The spectra we measured at the *K*-edge shown in Fig. 4 (right) are actually different from those available in the literature. The pre-edge peak *a* is not present in Kravtsova's spectrum (Kravtsova *et al.*, 2004) while it is probably present in a more recent contribution (Alonso Mori *et al.*, 2009). We point out here that the origin of the differences is the experimental resolution, which is significantly improved in the recent years.

Unlike the size effects observed at the Ca *K*-edge, the S *K*-edge spectra shows clear features in the larger clusters: (i) the long-range multiple scattering peaks *d*, *e* and *f* increase as the cluster size increases and become more pronounced in the non-MT approach; (ii) the white-line peaks, namely the features *b* and *c*, are enhanced in the large cluster within the non-MT approach; (iii) opposite to the Ca *K*-edge, the pre-edge peak (feature *a*) appears also in a relatively small cluster (*e.g.* 8 Å). However, the peak position agrees well with experimental spectra only when a large cluster and a non-MT potential is employed.

We have to mention here also that S atoms may exhibit several valences and easily react with X-ray radiation (Wilke *et al.*, 2008; Hackett *et al.*, 2012). As a consequence, the anomalous feature *f* cannot be explained without taking into account the complex valence state possibly owing to a charge transfer induced by radiation damage. This mechanism hampers the experimental determination of the sulfur valence and also poses a great challenge to the theoretical description. This work is mainly a comparison between MT and non-MT potentials and a further investigation of the sulfur valence states is left to a further work.

In this section we discussed potential effects and size effects in CaS. We have yet another tool to probe the system and better understand the CaS electronic structure. This tool is the orbital-projected density of states that reflects the population of atomic states available from different orbitals and atoms. It is a useful and important tool to recognize peaks and reconstruct details of the system electronic structure.

4.4. Projected density of states: the calcium *K*-edge

As discussed above, the pre-edge at the Ca *K*-edge in the CaS is complex and interesting owing to the possible interplay between electron hybridization and long-distance atomic scattering contributions. In Fig. 5 (left) we show the projected density of states and compare it with the theoretical spectrum at the Ca *K*-edge. From the comparison we may claim that the pre-edge feature *a* mainly originates from Ca *d* states hybridized with S *p* states, similarly to transition metal oxides where the hybridization of transition metal *d* states and oxygen *p* states drives the pre-edge behavior. Moreover, the hybridization also occurs between Ca *p* and *d*. The origin of features *b*, *c* and *d* can be assigned to the strong hybridization between Ca *p*, *d* states and S *p* states. Recently, Chen *et al.* (2007) calculated the band structure and the projected density of

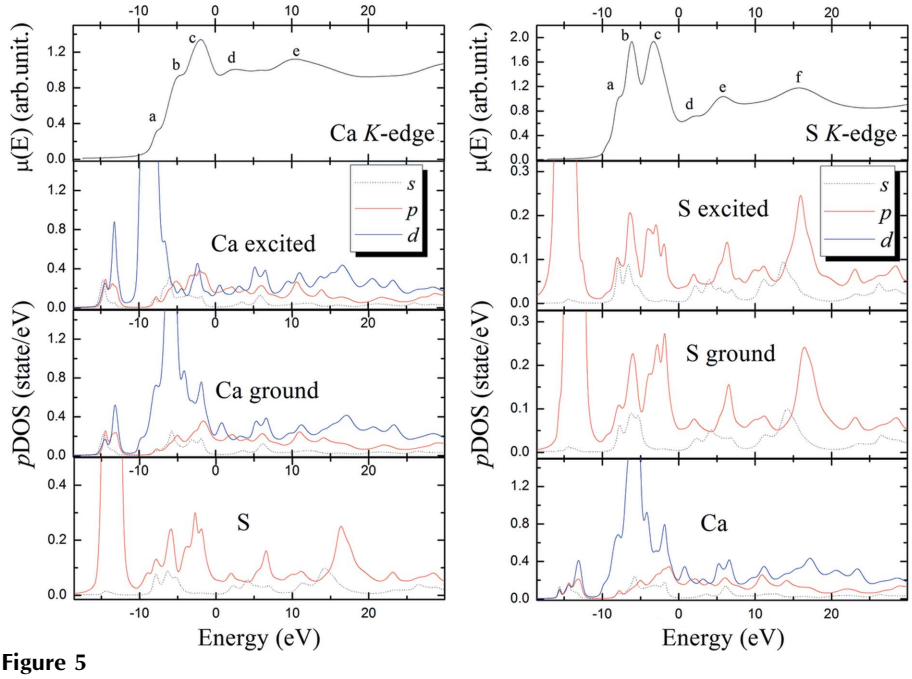

Figure 5
(Left) Comparison of the *l*-projected density of states and the Ca *K*-edge XANES spectrum (top). (Right) the same as in the left panel but for the S *K*-edge.

Table 2
Charge transfer and the *l*-projected charge values.

Edges	$\|\Delta e\|$	Ca *s*	Ca *p*	Ca *d*	S *s*	S *p*	S *d*
Ca *K*-edge	0.216	0.361	6.554	0.869	1.858	4.297	0.061
S *K*-edge	0.253	0.352	6.537	0.854	1.859	4.341	0.058

states using density functional theory. In their calculation the band structure shows a wide direct bandgap about 4.47 eV wide at the Γ point and the density of states indicated that Ca *d* states dominate at the Fermi energy. Our calculation shows a similar trend: (i) calcium *d* states are present at the Fermi level giving rise to the pre-edge feature; (ii) the sulfur *p* states dominate at energies about 5 eV below the Fermi energy. The density of states extracted from XANES calculations is then in agreement with first-principles calculations.

4.5. Projected density of states: the sulfur *K*-edge

In Fig. 5 (right) the projected density of states at the S *K*-edge is presented and compared with the theoretical XANES spectrum. Also in this case, it is evident that the edge structure (features *b* and *c*) originates from S empty *p* states. Furthermore, the features *d*, *e* and *f* also resemble *p* states of S atoms, pointing out the presence of strong electronic effects at the S *K*-edge. The pre-edge feature *a* is due to a strong hybridization between S *p* states and Ca *d* states, evident also at the Ca *K*-edge spectrum. The *s* states of sulfur partially contribute to the pre-edge feature of the S *K*-edge XANES spectrum. For the *p* states of sulfur, the largest density of states is around −10 eV on our energy scale, *i.e.* far away from the Fermi energy, as confirmed also by first-principles calculations (Chen *et al.*, 2007). These states are fully occupied and not available for electron transitions; as a consequence, no other features below the feature *a* can be observed.

As listed in Table 2, electronic parameters (the absolute charge transfer and charge counts for different atomic orbitals) have been compared at both Ca and S *K*-edges. The charge transfer is about 0.21–0.25 electrons while Ca *d* states have a large charge count (∼0.86 electrons), close to the value (0.855) of the CaO system (Modrow *et al.*, 2003), indicating similarity of the charge distribution in the two systems.

5. Conclusions

We have presented here the electronic structure of CaS, a simple system with a cubic structure but large interatomic distances. X-ray absorption spectra at the Ca and S *K*-edges have been measured and interpreted within the framework of the MST using both the MT potential and the finite-difference method without the MT approximation.

We found that, owing to the less compact structure of the CaS, both potential and size effects dominate either at both the Ca and the S *K*-edges. The hybridization between calcium *d* states and sulfur *p* states drives the structure of the pre-edge at both edges. Finally, the Fermi energy of the system mainly depends on Ca *d* electrons, implying that a strong electron correlation is present in this system. It is interesting to note that a similar behavior can be observed in transition metal oxides, in particular in terms of similar hybridization of states between cation *d* states and anion *p* states. Thinking about applications, CaS is a well known material in the luminescence technology. The hybridization between doped rare-earth metals and the element in the matrix compound influences the band structure near the gap, and thus the performance of devices that employ the hybridized materials. It is therefore interesting and promising to investigate *in situ* operation of the CaS-based luminescent devices, using the approach outlined in this contribution.

The project has been supported by the National Natural Science Foundation of China (grant No. 11105172). We thank Professor Y. Joly for many fruitful discussions.

References

Alonso Mori, R., Paris, E., Giuli, G., Eeckhout, S. G., Kavčič, M., Zitnik, M., Bučar, K., Pettersson, L. G. M. & Glatzel, P. (2009). *Anal. Chem.* **81**, 6516–6525.
Barrett, E., Fern, G. R., Ray, B., Withnall, R. & Silver, J. (2005). *J. Opt. A*, **7**, S265.
Chen, Z. J., Xiao, H. Y. & Zu, X. T. (2007). *Physica B*, **391**, 193–198.
Farrell, S. P., Fleet, M. E., Stekhin, I. E., Kravtsova, A., Soldatov, A. V. & Liu, X. (2002). *Am. Mineral.* **87**, 1321–1332.
Guo, Y. D., Yang, Z. J., Gao, Q. H., Liu, Z. J. & Dai, W. (2008). *J. Phys. Condens. Matter*, **20**, 115203.
Hackett, M. J., Smith, S. E., Paterson, P. G., Nichol, H., Pickering, I. J. & George, G. N. (2012). *ACS Chem. Neurosci.* **3**, 178–185.
Hakamata, S., Ehara, M., Kominami, H., Nakanishi, Y. & Hatanaka, Y. (2005). *Appl. Surf. Sci.* **244**, 469–472.
Hedin, L. & Lundqvist, S. (1970). *Solid State Physics*, Vol. 23, edited by D. T. Frederick Seiz and E. Henry, pp. 1–181. New York: Academic Press.
Joly, Y. (2001). *Phys. Rev. B*, **63**, 125120.
Kravtsova, A., Stekhin, I., Soldatov, A., Liu, X. & Fleet, M. (2004). *Phys. Rev. B*, **69**, 134109.
Luo, H., Greene, R. G., Ghandehari, K., Li, T. & Ruoff, A. L. (1994). *Phys. Rev. B*, **50**, 16232.
Modrow, H., Bucher, S., Rehr, J. J. & Ankudinov, A. L. (2003). *Phys. Rev. B*, **67**, 035123.
Moreno, M. S., Jorissen, K. & Rehr, J. J. (2007). *Micron*, **38**, 1–11.
Natoli, C. R., Benfatto, M., Della Longa, S. & Hatada, K. (2003). *J. Synchrotron Rad.* **10**, 26–42.
Norman, J. G. (1974). *Mol. Phys.* **81**, 1191–1198.
Rao, R. (1986). *J. Mater. Sci.* **21**, 3357–3386.
Ravel, B. & Newville, M. (2005). *J. Synchrotron Rad.* **12**, 537–541.
Rehr, J. J. & Albers, R. C. (2000). *Rev. Mod. Phys.* **72**, 621–654.
Rehr, J. J., Kas, J. J., Prange, M. P., Sorini, A. P., Takimoto, Y. & Vila, F. (2009). *C. R. Phys.* **10**, 548–559.
Shaukat, A., Saeed, Y., Ikram, N. & Akbarzadeh, H. (2008). *Eur. Phys. J. B*, **62**, 439–446.
Versluys, J., Poelman, D., Wauters, D. & Meirhaeghe, R. L. V. (2001). *J. Phys. Condens. Matter*, **13**, 5709.
Wilke, M., Jugo, P. J., Klimm, K., Susini, J., Botcharnikov, R., Kohn, S. C. & Janousch, M. (2008). *Am. Mineral.* **93**, 235–240.
Xu, W., Chen, D., Chu, W., Wu, Z., Marcelli, A., Mottana, A., Soldatov, A. & Brigatti, M. F. (2011). *J. Synchrotron Rad.* **18**, 418–426.